nature electronics

Article

https://doi.org/10.1038/s41928-024-01268-z

Soft electronic vias and interconnects through rapid three-dimensional assembly of liquid metal microdroplets

Received: 13 November 2023

Accepted: 26 September 2024

Published online: 24 October 2024

Check for updates

Dong Hae Ho [1,2,4], Chenhao Hu [3,5], Ling Li [3,5] & Michael D. Bartlett [1,2]

The development of soft electronics requires methods to connect flexible and stretchable circuits. With conventional rigid electronics, vias are typically used to electrically connect circuits with multilayered architectures, increasing device integration and functionality. However, creating vias using soft conductors leads to additional challenges. Here we show that soft vias and planar interconnects can be created through the directed stratification of liquid metal droplets with programmed photocuring. Abnormalities that occur at the edges of a mask during ultraviolet exposure are leveraged to create vertical stair-like architectures of liquid metal droplets within the photoresin. The liquid metal droplets in the uncured (liquid) resin rapidly settle, assemble and then are fully cured, forming electrically conductive soft vias at multiple locations throughout the circuit in a parallel and spatially tunable manner. Our three-dimensional selective stratification method can also form seamless connections with planar interconnects, for in-plane and through-plane electrical integration.

To create highly integrated circuits[1], multiple circuit layers can be connected with vias that electrically interconnect different layers[2]. For traditional, rigid electronics the fabrication of vias is well established. Silicon wafer level vias in micro-to-nanometre regions are created through chemical or plasma etching, and larger scale printed circuit board vias are made with micro or laser drilling followed by electroplating or filling with conductive materials[3].

For soft electronics—which are of use in soft robotics[4–6], wearable electronics[7–10] and flexible displays[11–13]—integration approaches and multilevel architectures are undeveloped compared with their rigid counterparts. The primary role of vias is to electrically connect different layers, but soft devices introduce several new challenges due to their mechanically dynamic and conformal nature. First, due to the mechanics of flexible substrates, vias can act as stress concentration points that induce structural flaws[14]. Second, rigid metallic vias in stretchable substrates can cause mechanical failure due to the modulus mismatch between the substrate and the vias[15,16]. Third, current fabrication techniques for creating vias typically involve a time-consuming multistep procedure such as epoxy resin or copper composite filling or electroless plating[17–19]. In addition, via fabrication in flexible electronics still relies on two-dimensional manual drilling procedures that are performed for every individual via. Therefore, while soft electronics has advanced notably in-plane, through-plane integration presents challenges.

One approach to address these challenges is to use stretchable and flexible conductive materials, such as liquid metal (LM). LM has a combination of fluidity and high thermal and electrical conductivity[20–24], allowing it to be used as an electrically conductive material in various flexible and stretchable electronics[25–27]. In addition, LM-based composites can incorporate high electrical and/or thermal conductivity into soft polymers[28–32]. LM has been used as a via material using various methods, including wetting or filling of the via holes[33–37], lift-off

[1]Department of Mechanical Engineering, Soft Materials and Structures Lab, Virginia Tech, Blacksburg, VA, USA. [2]Macromolecules Innovation Institute, Virginia Tech, Blacksburg, VA, USA. [3]Department of Mechanical Engineering, Virginia Tech, Blacksburg, VA, USA. [4]Present address: Department of Energy Science and Engineering, Daegu Gyeongbuk Institute of Science and Technology (DGIST), Daegu, Republic of Korea. [5]Present address: Department of Materials Science and Engineering, University of Pennsylvania, Pennsylvania, PA, USA. e-mail: mbartlett@vt.edu

patterning[38] and using iron wires to make the through-hole and wetting it with LM[39]. However, these methods include multistep via fabrication techniques that make individual holes using templates or drilling procedures, which are limited to the two-dimensional domain. LM filling techniques can also have interface problems. For example, the surface of the LM interconnect can be easily disturbed by physical deformation. Integrating LM with conventional solid electronic components can also cause bonding issues between the substrate and the solid electronics due to the fluidic nature of LM.

In this Article, we report a LM programmed stratification technique to form soft vertical vias and planar interconnects between and across circuit layers. The process uses ultraviolet (UV)-curable photoresin containing dispersed LM microdroplets (LMMDs) as the circuit material. Placement of the LM throughout the circuit volume is controlled by using a shadow mask to vary the exposure to UV light. Photoresin exposed to UV solidifies and LMMDs are fixed in place, while in areas not exposed the photoresist remains a liquid and LMMDs, which have a higher density, sink to the bottom. Our approach relies on an imperfect curing anomaly that occurs at the edges of the shadow mask, where the photoresin receives a smaller UV expose dose than centre regions and is only partially cured, to create a stair-like structure. The stair-like structure in the photoresin acts as a foundation for programmed settling and assembly of LM droplets, creating a continuous trace of LMMDs from the top to the bottom layer (Fig. 1a and Supplementary Video 1). This phenomenon occurs in under 1 minute and can create hundreds of vias across the plane simultaneously. Our approach—which we term liquid metal stratification for three-dimensional (3D) assembly of electrical interconnects (LM-STAIR)—is a rapid and scalable technique to create 3D interconnected circuit designs in soft and flexible electronics.

In contrast to conventional via approaches, such as through-hole and wire bonding, LM stratification creates multilayer circuits without through holes or bond lines, forming robust connections in continuous films (Fig. 1b). Our approach offers desirable mechanical and electrical properties for soft and flexible devices, including tunable modulus and strain invariant electrical conductivity. We show that the approach can be used to connect several circuits, including a hybrid electronic device that incorporates magnetic field sensing and display functions on a single, double-sided device.

3D assembly of LM-STAIR soft vias

The curing behaviour of photoresin enables LM-STAIR to create a continuous electrical path from the top to the bottom layer. Our approach is governed by two phenomena. First, selective curing of the photoresin. When the photoresin and/or diluent and LMMDs composite is exposed to UV, the photoresin solidifies and the position of LMMDs are fixed within the cured region. However, areas not exposed to UV remain in the liquid state, allowing LMMDs to move freely inside the liquid-state photoresin. LMMDs have a higher density (6.25 g cm^{-3}) compared to the photoresin (1.05 g cm^{-3}), so LMMDs in the uncured region can sediment due to gravity. Second, undercut behaviour occurs at the edge of the shadow mask. When photoresin is exposed to UV, the curing reaction is focused in the centre of the exposed area rather than the edges, which results in a convex curing profile (Supplementary Fig. 1)[40]. The slope of the convex profile provides a 3D foundation for the LMMDs to settle and creates a continuous droplet film from the top to the bottom plane (Fig. 1c, right). The LMMDs are then electrically activated through the application of mechanical pressure to percolate the droplets and form a continuous conductive network. Other activation techniques, such as the use of acoustic fields[30,32], can also be used to activate the LM networks, as shown in Supplementary Fig. 2 and Supplementary Video 2. By combining these two phenomena, we created a flexible double layer circuit where two different planes are electrically connected without a through-hole (Fig. 1d). The presented sample circuit has parallel top and bottom planar interconnects that cross each other without causing a short circuit, resulting in illumination of both light-emitting diodes (LEDs) on the top and bottom sides of the plane. This parallel, two-level LM-STAIR fabrication method will be discussed further in a later section.

Directed stratification of LMMDs is presented in real time in Fig. 1c (left) and Supplementary Video 3. As shown in the photograph at 5.17 s, LMMDs inside the cured area are fixed in position while LMMDs inside the uncured photoresin stratify to the bottom, resulting in directed stratification and 3D control of LMMD connectivity. In contrast, previous LM composites that use sedimentation required long times (due to viscosity) and only focused on homogeneous settlement (that is, the droplets settled throughout the entire composite)[28,29]. Our technique uses heterogeneous and selective stratification that results in controlled 3D droplet architectures. One of the enabling aspects of LM-STAIR is that the LMMD stratification is completed in less than 1 minute and is not affected by the number and size of the vias. Therefore, the complexity of the circuit does not affect the processing time, unlike through-hole processes that create vias individually. Thus, the method is scalable with a short processing time and large areal coverage. To demonstrate this, ten linear stencil-printed LMMD planar interconnects were turned into 200 3D-structured vias through LM-STAIR in less than 1 minute (Fig. 1e and Supplementary Fig. 3).

Mechanical characterization of LM-STAIR

The photoresin is composed of acrylate and methacrylate-based polymer, and dibutyltin dilaurate (Fig. 2a). Adding a diluent, aliphatic monofunctional acrylate, softens the cured photoresin[41]. The weight percentage (wt%) of the diluent with the photoresin is modified to control the mechanical properties and the ratio will be designated as 30:70, for example, 30 wt% of the photoresin and 70 wt% of the diluent. The volume fraction of LMMDs are quantified by ϕ, where ϕ is volume of LMMDs/volume of (LMMDs + photoresin + diluent).

LMMDs are created using a shear mixing process (Fig. 2b, left schematic), where a single large drop of LM in uncured photoresin breaks into LMMDs. The effect of shear mixing speed on the size of the LMMDs is measured by performing an image analysis on optical micrographs (Supplementary Fig. 4). The results indicate that the LMMD diameter plateaus at approximately 100 µm for the mixing condition of 2,000 rpm after 2 minutes of mixing. Using a different combination of diluent and viscosity modifier, smaller LMMD sizes can be achieved to decrease the minimum electrode width of the circuit electrodes (Fig. 2c). We choose a shear mixing setup (2,000 rpm, 2 minutes) that can produce the smallest LMMDs for the rest of the experiments.

To determine the appropriate polymer matrix for the LM-STAIR via, the elastic modulus of the photoresin or diluent without LMMDs is first measured (Fig. 2d and Supplementary Figs. 5 and 6). The elastic modulus of the cured pristine photoresin (100:0, ϕ = 0%) is measured as 1,100 MPa, which is higher than most soft and stretchable electronics (50 kPa–3 MPa)[42,43]. Through the addition of diluent, the modulus of the polymer matrix decreases to 35 MPa (50:50, ϕ = 0%) and further to 2 MPa (10:90, ϕ = 0%). To make flexible and stretchable electric circuits, formulations containing ≤50 wt% photoresin are chosen to test elastic modulus of the composite that includes LMMDs.

To understand the effect of LMMDs in the polymer matrix, the elastic modulus is measured for the planar line shape interconnect (planar interconnect) and the LM-STAIR via (Fig. 2d). The results indicate that the inclusion of LMMDs causes a slight decrease in elastic modulus, which is consistent with the typical response when liquid fillers are added to a polymer or elastomer matrix[44,45]. In addition, the type of interconnect does not show any large difference in elastic modulus. The strain at break for the selected samples is obtained from the same test. For a planar interconnect, the strain at a break of ϕ = 10% and 20% LM shows 23.6 ± 0.8 and 20.0 ± 5.3%, respectively (Fig. 2e and Supplementary Fig. 7). These values are higher than the ϕ = 0% LM sample of 17.7 ± 2.5%, showing that LMMDs do not degrade and potentially can improve the mechanical properties. LM-STAIR vias show a similar

https://doi.org/10.1038/s41928-024-01268-z

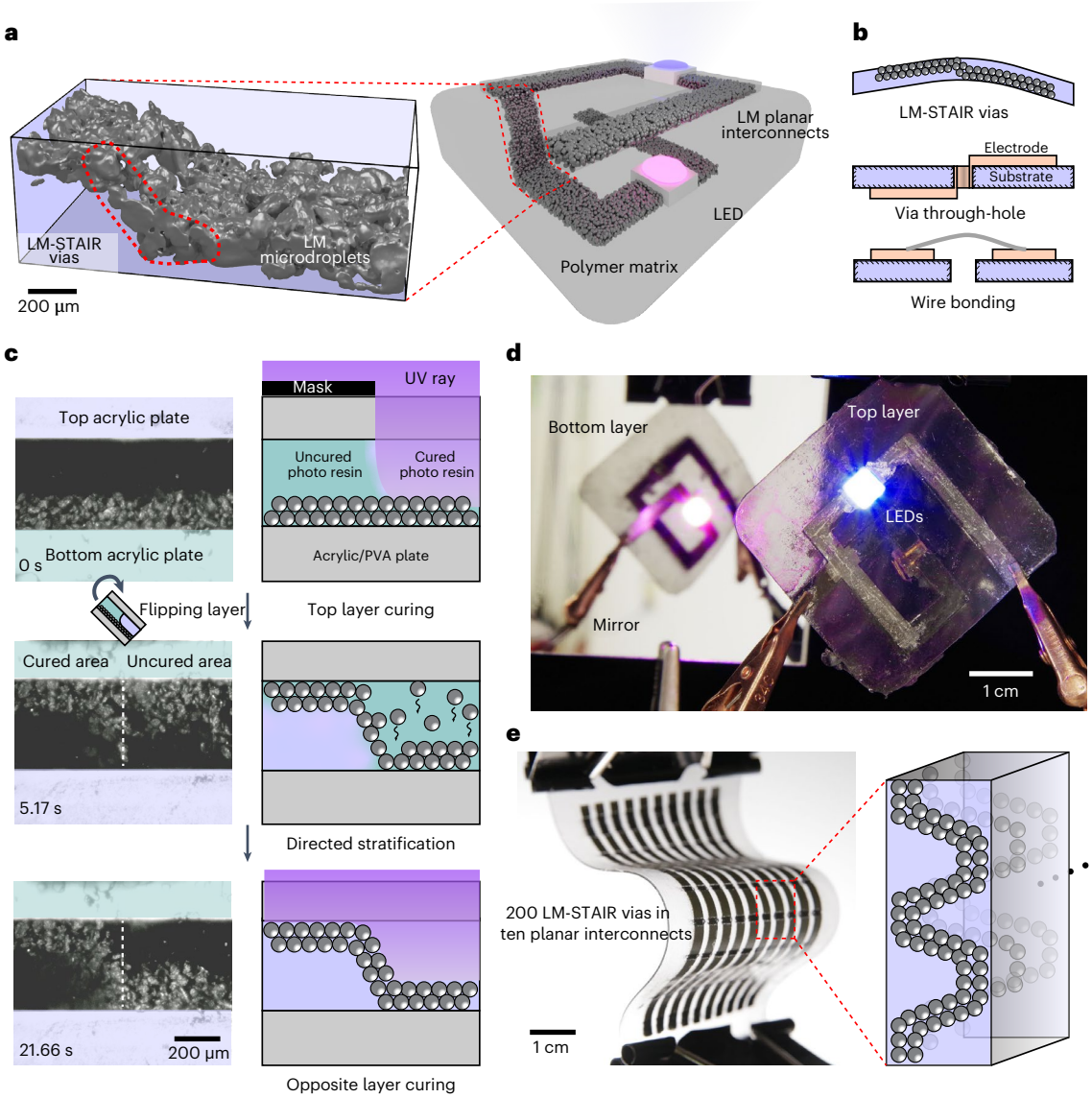

Fig. 1 | LM-STAIR fabrication of LM soft interconnects and vias. **a**, Reconstructed microCT scan of LM-STAIR vias (left) and a schematic of a circuit that includes LM-STAIR vias seamlessly connecting top and bottom planar interconnects. **b**, Diagrams of representative electrical connection methods between two different planes. **c**, Images (left) and schematics (right) showing the directed stratification process of LMMDs. **d**, A functional circuit that includes a via junction and crossing top and bottom layer planar interconnects created through the LM-STAIR process. **e**, Photograph of a sample with 200 LM-STAIR vias in ten planar electrodes and a diagram of LMMDs in the polymer matrix.

strain at a break of 16.8 ± 3.0% at ϕ = 20% LM compared to the non-LM photoresin (17.7 ± 2.5%).

Micro-computed tomography (microCT) scans of the planar interconnect are taken to characterize the effective volume fraction of LM in the composite (Supplementary Fig. 8a). The LM volume fraction inside the composite is calculated from the reconstructed microCT image (Supplementary Fig. 8b). The planar interconnect has ϕ = 16.4% LMMDs inside the path, while the LM-STAIR via has ϕ = 14.5% LMMDs. Although the effective volume fraction of LMMDs is smaller than that of other LM-based composites ($\phi \geq 50\%$)[29,46,47], because of the confined concentration, it is possible to create a percolated conductive network at lower loadings of LMMDs.

To confirm this, the percolation network formation is observed by microCT (Fig. 2f and Supplementary Video 4). The LMMDs are percolated using a mechanical embossing method (that is, activation process) that applies pressure to rupture the LMMDs and connect them (Supplementary Fig. 9). In Fig. 2f, each colour denotes a cluster that can be defined as a single connected droplet network. We find that the unactivated sample is a collection of individual or small clusters of droplets, however, the nearly single-coloured image of the activated sample shows that most of the LMMDs are connected as a single percolated conductive network. To quantify the connectivity of the unactivated and activated composite, the individual volume fraction of every cluster is graphed out (Fig. 2g). The result shows that the largest cluster of unactivated droplets occupies 20% of the total 3D reconstructed volume, representing a discrete network. However, the largest cluster for the activated droplets occupies 99.3% of the total volume, which is indicative of a single continuous network.

We further examine the microCT data through percolation network analysis. The activated and unactivated samples are segmented into individual particles using the random-walk distance transforms (Supplementary Fig. 10)[48]. The unactivated sample shape factor (shape factor $= \frac{\text{surface area}^3}{36\times\pi\times\text{volume}^2}$, where a perfect sphere is 1) shows a smaller distribution and lower average values compared to the activated samples, indicating that the activation process breaks the spherical shape

https://doi.org/10.1038/s41928-024-01268-z

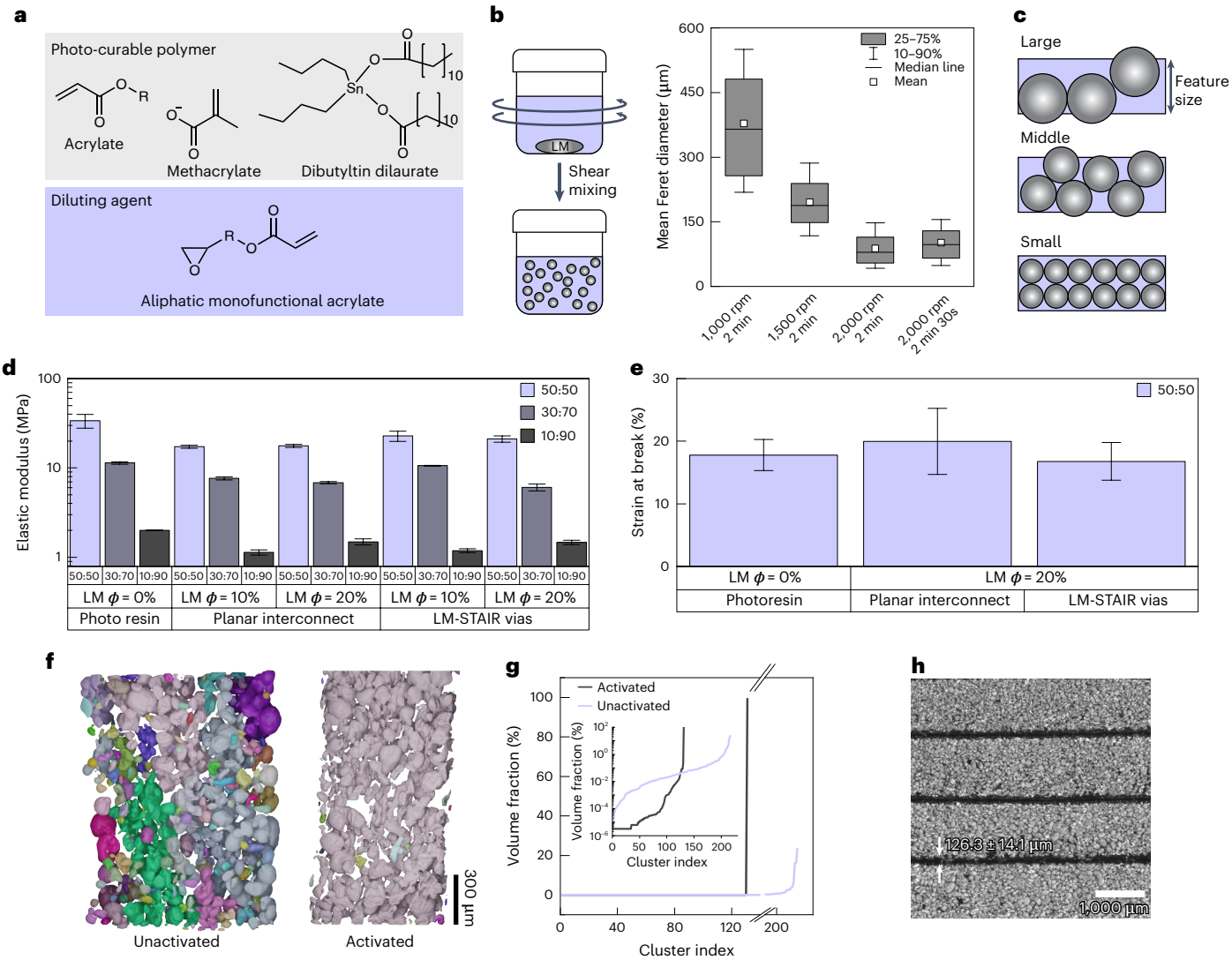

Fig. 2 | Physical characterization of LM-STAIR vias and interconnects. **a**, Chemical structure of the photocurable polymer and diluting agent. **b**, Analysis of LMMDs size based on shear mixing rpm and processing time. Data are collected from individual LMMD Feret diameters, and the number of droplets for each bar is 41, 133, 448 and 493 (from left to right order). Data are presented as mean values ± standard deviation (s.d.). **c**, Diagram of circuit feature size based on LMMD diameter. **d**, Young's modulus based on different ratios of photoresin, diluent and LM volume percentage. The ratios in the legend represent the weight ratio of photoresin and diluent (for example, 30:70 denotes 30 wt% of photoresin and 70 wt% of diluent). LM is added to the uncured photoresin and diluent as the total volume percentage of the composite. **e**, Strain at the break based on different ratios of photoresin, diluent and LM volume percentage. Data in **d** and **e** are presented as the mean ± s.d. ($n = 3$ measurements from distinct samples). **f**, Reconstructed microCT images of unactivated and activated samples. **g**, The volume fraction analysis for each cluster. **h**, Optical microscopic image of the minimal gap between electrically conductive planar interconnects.

of the LMMDs and transforms them to a more irregular shape (Supplementary Fig. 10a). Additionally, the coordination number, which refers to the number of connections between different LMMDs, increases as a result of activation (Supplementary Fig. 10b). Furthermore, Supplementary Fig. 10c shows that larger LMMDs tend to locate at the bottom of the composite and have a higher coordinate number, which agrees with Stoke's law that larger LMMDs have a higher settling velocity[49]. Also, larger LMMDs tend to form more connections due to their higher number of neighbouring LMMDs. Taken together, these results show the LM-STAIR fabrication approach supports the formation of a controlled, 3D network of connected LMMDs, and presents quantitative morphological evidence for LM network formation in general.

In addition, the minimum feature size of the stencil mask patterning method is investigated. As shown in Fig. 2h and Supplementary Fig. 11, the minimum gap between planar interconnects and the minimum width of the planar interconnect are 126 and 208 μm, respectively. The electrical resistance of the minimum feature size planar interconnect (5 cm length) is measured to ensure that the LMMDs are electrically connected to each other (Supplementary Fig. 12). Electrical isolation between each planar interconnect is measured to ensure that traces are conductive but isolated from each other (Supplementary Fig. 13). The resolution of the stencil mask patterning method can be further improved using a more advanced stencil fabrication method and smaller LM droplets in the future. We further examine the applicability in four different acrylic and silicone-based photoresins. As shown in Supplementary Fig. 14, vias are successfully fabricated in all the resins, presenting the generalizable nature of our method.

Electromechanical characterization of LM-STAIR

Along with the physical characteristics, the electromechanical properties of the fabricated samples are determined. During the electromechanical test, a 50:50 photoresin–diluent polymer matrix is used. To measure the electromechanical response, dog-bone samples with a

https://doi.org/10.1038/s41928-024-01268-z

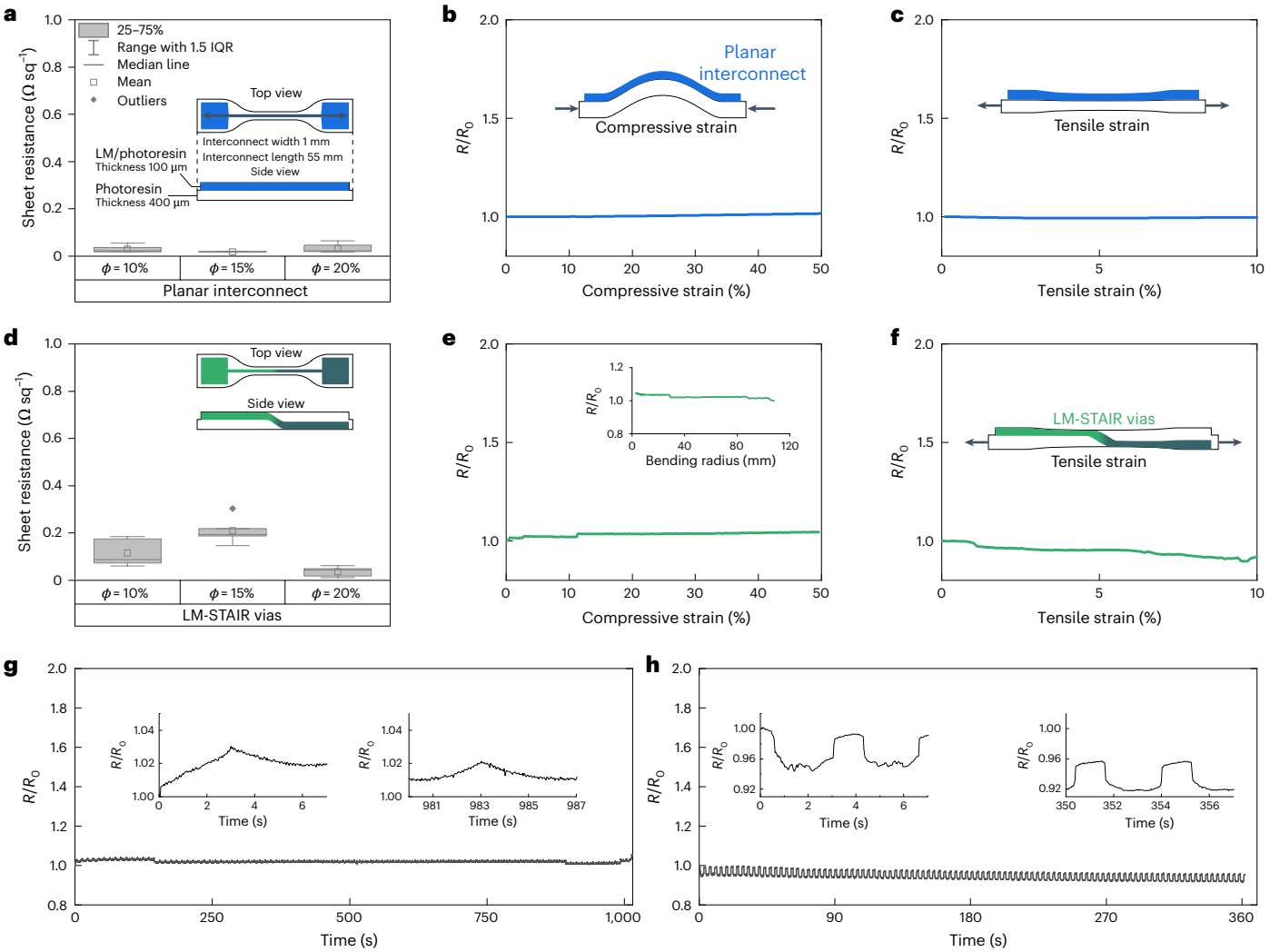

Fig. 3 | Electromechanical characterization of LM-STAIR vias and interconnects. a, Sheet resistance of the planar interconnect flexible circuit based on the three different LM volume percentages ($n = 5$ measurements from distinct samples). **b**, Relative electrical resistance of the planar interconnect flexible circuit according to the compressive strain. **c**, Relative electrical resistance of the planar interconnect flexible circuit depending on the tensile strain. **d**, Sheet resistance of LM-STAIR vias based on the three different percentages of LM volume ($n = 5$ measurements from distinct samples). The definition of the box plot is the same as **a**. **e**, Relative electrical resistance of the LM-STAIR via flexible circuit depending on compressive strain. The inset shows the resistance behaviour, depending on the measured bending radius of the specimen. **f**, Relative electrical resistance of the LM-STAIR vias flexible circuit depending on the tensile strain. **g**, Durability test of the LM-STAIR vias flexible circuit for 100 cycles of compressive strain 50%. The inset shows the initial and final 7 s of the cycle. **h**, Durability test of the flexible LM-STAIR via circuit for 100 cycles of 50% tensile strain. Inset shows the initial and final 7 s of the cycle.

single planar interconnect are fabricated (Fig. 3a, inset). First, the sheet resistance of the planar interconnects $\phi = 10$, 15 and 20% LM samples are measured and all samples show less than 0.1 Ω sq^{-1} (Fig. 3a). The electromechanical response of the $\phi = 20\%$ LM sample during bending (50% compressive strain) and uniaxial tension (10% strain) is also measured. During the test, the relative electrical resistance maintains a constant level of one during both bending (Fig. 3b) and tension (Fig. 3c).

The LM-STAIR vias with $\phi = 10$, 15 and 20% LM are measured in the same manner as the planar interconnect (Fig. 3d). The sheet resistance of the LM-STAIR via is less than 0.3 Ω sq^{-1}, which is slightly higher compared to the planar interconnects. This is attributed to the longer path length and the lower volume fraction of the LM-STAIR via region, as shown in the inset of Fig. 3d and Supplementary Fig. 8. Compressive and tensile strain tests are performed with LM-STAIR via samples (Fig. 3e,f). During the compressive strain test, the bending radius is measured (inset of Fig. 3e). The minimum bending radius is 3.17 mm, and its relative electrical resistance remains constant throughout the test. The tensile test up to 10% strain also showed a consistent electromechanical response. These results show that the via is robust and can withstand different modes of deformation, including folding and stretching. We further examine the electromechanical durability of the vias with 100 cyclic strain tests that include 50% compressive strain and 10% tensile strain. From both types of strain test, LM-STAIR via exhibit a consistent electromechanical response (Fig. 3g,h).

After electromechanical characterization, the dielectric constant of the cured photoresin and/or diluent without LMMDs is measured. The dielectric constant is a critical factor for signal integrity and impedance matching to make a high-performance electric circuit[50]. The measured dielectric constant is in the range of 3.5 to 4.3 (frequency range of 0.1 to 100 kHz, Supplementary Fig. 15). Considering that the dielectric constant of polyimide that is widely used in flexible commercial electronics is between 3.1 and 3.6, the current polymer matrix is suitable for a substrate material for a high-performance electrical circuit[51]. Further, environmental stability of the electrical resistance of a LM-STAIR via is examined without any additional encapsulation under two different conditions: (1) 80 °C elevated temperature and (2) 45 °C underwater

https://doi.org/10.1038/s41928-024-01268-z

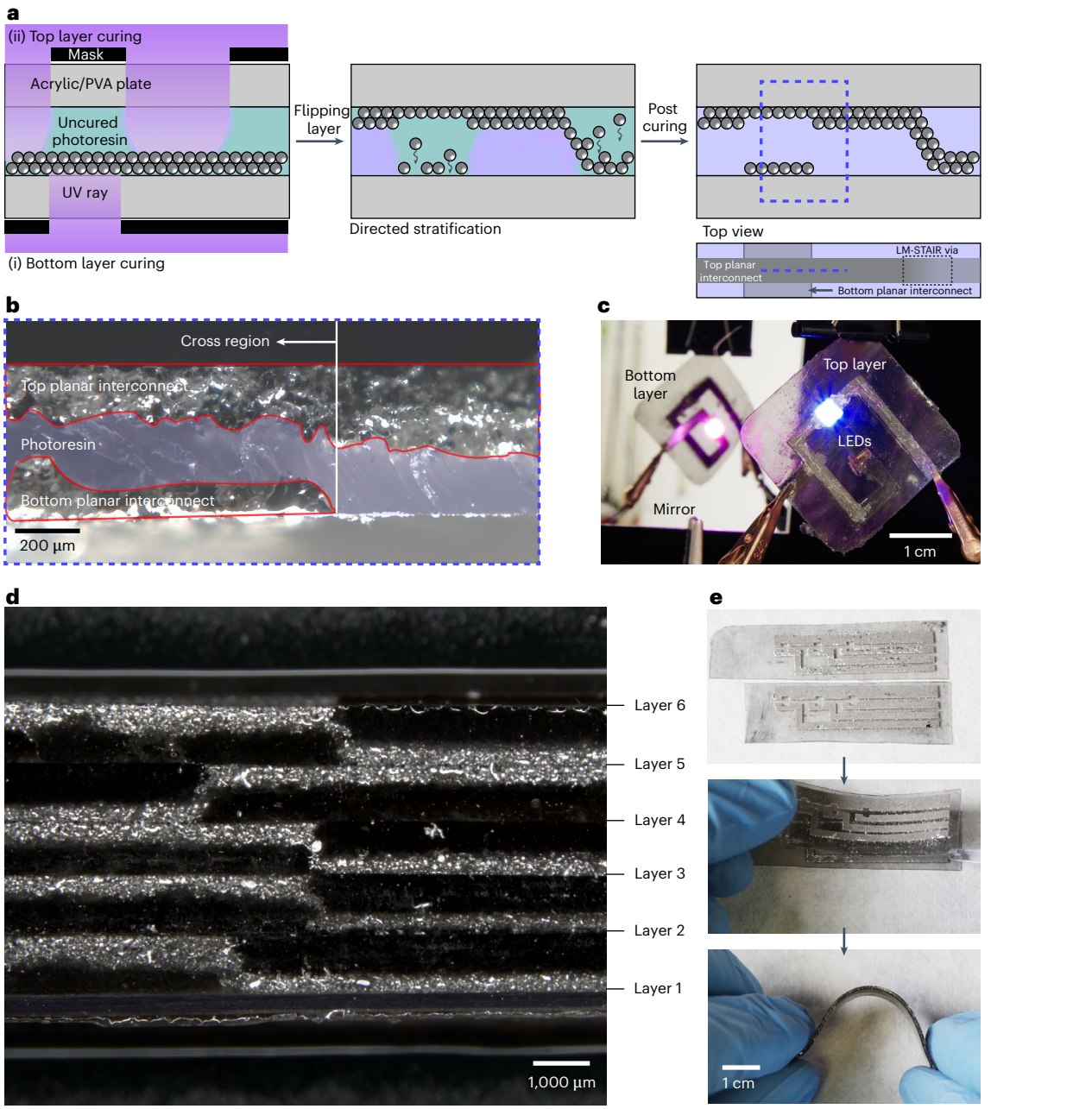

Fig. 4 | Multilayer circuit fabrication with crossing interconnects and adhesion characteristics. a, Diagram of the cross pattern and LM-STAIR via fabrication. **b**, Cross-sectional optical microscopic image of the cross pattern. The left half of the image is the cross-pattern region. The red dotted area represents the LMMD layers, and the blue shaded area represents photoresin. **c**, Fabricated LED circuit using a crossing pattern. **d**, Cross-sectional optical microscopy of six soft circuit layers with five vias in a single device. **e**, Manual bending test of a pair of adhered LM-STAIR circuits.

(tapwater) (Supplementary Fig. 16). Over 7 days in 80 °C, a slight decrease is observed in normalized resistance ($R/R_0 = 0.87 \pm 0.12$), while in the underwater sample the resistance increases slightly on the first day then stabilizes ($R/R_0 = 1.31 \pm 0.27$). This agrees with recent work that has shown the stability of LM-based soft composites in adverse underwater environments[52], and could probably be further improved with encapsulation if needed. The electromechanical tests results show that our technique can form and maintain robust electrical interconnections for reliable and flexible circuits.

Multilayer circuit fabrication with 3D interconnects

The LM-STAIR technique successfully creates electrical connections across circuit layers. Through this approach, we can also independently control the circuit layout within multiple layers and control connectivity across these layers. To achieve this, we modified the curing direction and sequence to specifically discretize a single layer of LMMDs into multiple layers. This allows planar interconnects to be created that can cross each other in difference layers or planes without being electrically connected except at specified locations where the LM-STAIR method places soft vias (Fig. 4a)

First, we created a single crossing planar interconnect by partially UV curing through the LMMD layer (that is, UV exposes through the bottom side) (Fig. 4a(i), bottom layer curing). As LMMDs act as UV blockers, the curing of the photoresin is limited to a shallow depth. As a result, this only partially cures the layer of LMMDs. The LMMDs at a greater depth remain in uncured photoresin, which act as the source of LMMDs for the second crossing planar interconnect.

https://doi.org/10.1038/s41928-024-01268-z

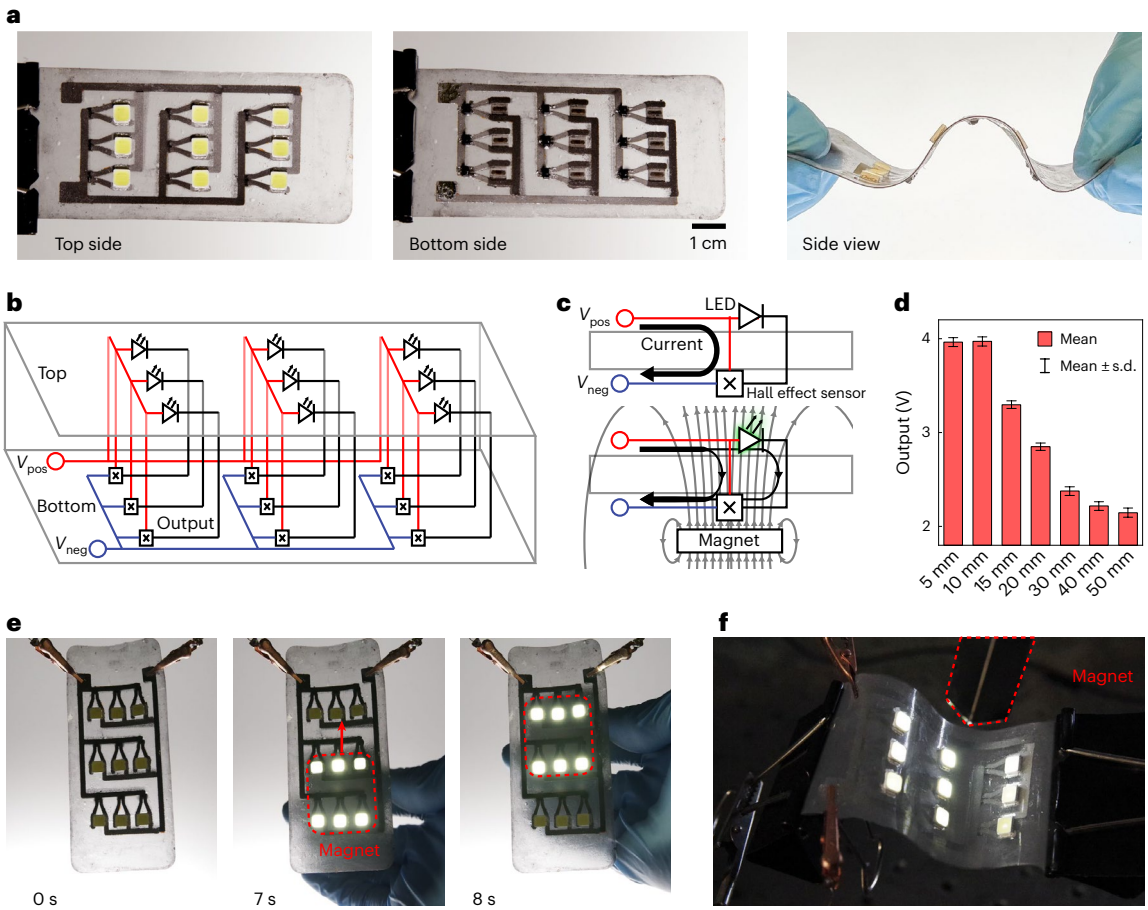

Fig. 5 | Multilayer magnetic sensing and indicating flexible circuit demonstration. a, Photographs of the magnet sensing and indicating flexible circuit made through the LM-STAIR approach. **b**, Circuit diagram of the magnet sensing and indicating flexible circuit. **c**, Diagram of the Hall effect sensor working mechanism. **d**, Output of the Hall effect sensor depending on the distance of a magnet from the Hall effect sensor. Data are presented as mean ± s.d. for 14,000 data points equivalent to 1.4 s. **e**, Photographs of the LEDs illuminated by varying the position of a magnet behind the flexible circuit. **f**, Photograph of the flexible circuit deformed and still functioning as a magnet approaches.

The UV exposure time can be used to control this discretization process. Too much curing time locks nearly all LMMDs into the upper position while too little curing time does not lock hardly any LMMDs into the upper position, while an intermediate curing time can stratify a single layer of LMMDs into multiple layers (Supplementary Fig. 17). Next, the top side is exposed to UV with a shadow mask placed in the region where the top and bottom planar interconnects will cross (Fig. 4a(ii), top layer curing). During this step, the crossing region is still partially uncured. Then, the LMMDs in the uncured areas (the crossing region and unexposed regions) of the composite are directionally stratified by flipping the layer upside down, while the cured part in the crossing region remains in position. Finally, the entire composite is cured. A cross-sectional micrograph in Fig. 4b shows the separation between the top and bottom planar interconnects as a result of this process. The cross-pattern fabrication method is demonstrated with an LED circuit with a cross pattern (Fig. 4c). The top and bottom layers of the circuit are illuminated by blue and red LEDs, respectively. This shows the effective creation of crossing planar interconnects, soft vias, and independent control of the circuit layout in multiple layers through the LM-STAIR methodology. This technique allows for the fabrication of intricate intertwined flexible circuits with high complexity. Furthermore, we developed a sequential LM-STAIR technique to create an arbitrary number of soft circuit layers by combining top and bottom curing (Supplementary Fig. 18). Following the normal curing procedure and stratification, by adding another layer of uncured LMMDs and/or photoresin followed by sequential top and bottom curing, six soft circuit layers with five vias were successfully created within a single device structure (Fig. 4d).

In addition to the ability to make 3D interconnects, the fabricated flexible circuit can also be stacked together through intrinsic adhesion. The low-modulus surface of the flexible circuits allows for reversible adhesion characteristics. To demonstrate this, two different LM-STAIR fabricated circuits are stacked together (Fig. 4e and Supplementary Video 5). The stacked circuits are flexed with no signs of detachment (Supplementary Fig. 19), indicating sufficient adhesion strength to maintain the bond between each layer. After the bending test, the stacked circuits can be intentionally separated by initiating a crack at an edge and then peeling apart (Supplementary Fig. 20). This adhesion characteristic could be a promising approach for stacking multiple flexible circuits in the future.

Multilayer dual function flexible circuit demonstration

The proposed LM-STAIR vias can electrically connect two different circuit planes in a simple manner. We demonstrate this by fabricating a flexible magnetic field sensing circuit with an embedded and interconnected indication circuit. The fabricated flexible circuit has two different layers; a top layer with nine white LEDs to indicate the magnitude of the magnetic field and a bottom layer with nine Hall effect sensors to sense the magnetic field (Fig. 5a). Hall effect

sensor outputs are individually connected to the top layer LED cathode through LM-STAIR vias. Connections between the soft circuit and rigid components are made with a paste formed from LM and Cu particles (Supplementary Fig. 21). Even with the complex connection of the electrical components, the thickness of the flexible circuit remained thin (0.33 mm). A total of 21 LM-STAIR soft vias and ~52 cm long planar interconnects are made (12 vias for the cathodes and nine for the outputs, Fig. 5b). These LM-STAIR vias seamlessly integrate two different functions. The circuit's on and off state is depicted in the Fig. 5c schematic. If there is no magnetic field, the Hall effect sensor output is half the applied voltage (4 V) (Fig. 5d). When a magnet is placed 50 mm from the Hall effect sensor, the output is ~2.1 V. At low output voltage, the connected LED does not turn on due to the minimum threshold voltage of the LED (3.2 V). After the Hall effect sensor output exceeds the LED threshold voltage, the LED lights up, as shown in the diagram at the bottom of Fig. 5c. To demonstrate the fabricated circuit, a rectangular magnet is placed beneath the circuit and moved from the bottom to the top of the circuit (Fig. 5e and Supplementary Video 6). It can be observed that only the LEDs near the magnet turn on. Furthermore, the fabricated circuit is bent in an S shape to illustrate the robust and soft electrical connections of LM-STAIR vias and planar interconnects (Fig. 5f and Supplementary Video 6). The bent circuit consistently performs both magnetic field sensing and indicating functionalities. From these demonstrations, the LM-STAIR methodology shows consistent electrical and electromechanical responses, and seamlessly connects two different circuit planes, forming both planar interconnects and soft vias.

Conclusions

We have reported a selective photocuring and programmed settling of LM particles fabrication method to rapidly create soft 3D interconnects (soft vias and planar interconnects) between different circuit planes. The approach offers a tunable, versatile and rapid manufacturing process to advance the in-plane and through-plane integration of soft and flexible electronic devices. Multilayer circuits connected with the technique exhibit high electrical conductivity and mechanical stability, and provide direct electrical and mechanical integration throughout the circuit volume without holes or secondary processes. Because the approach relies on the flow and curing characteristics of the photoresin to position LMMDs throughout the volume, a diverse range of photocurable materials can be used. There is a similar freedom of choice in the LM composition, which can be tuned by a variety of dopants or inclusions for different applications, for example, using iron-doped LM to enable a magneto-responsive composite. As such, future work could leverage a range of different chemistries or inclusion characteristics to broaden the functionality, including responsive systems, biocompatible or biodegradable materials, and multi-material systems.

One challenge that may arise within materials selection is the effect of functional inclusions on the photoresin viscosity. As increased loading of inclusions typically increases viscosity, this could require longer times for the particles to settle. This could be supplemented with techniques to accelerate particle settling, such as using a centrifuge or increasing the temperature to reduce viscosity. However, the programmed stratification technique effectively concentrates inclusions. Therefore, low inclusion loading before processing become more concentrated during processing, which maintains a working viscosity for rapid processing. Additional topics for future research include down-scaling of feature size through the use of higher resolution patterning methodologies, such as photolithography or e-beam lithography. It may also be possible to automate the fabrication steps to enable mass production of the multilayer soft electronic devices. Thus, the LM-STAIR methodology, and the resulting materials, can provide a basis for developing integrated soft and flexible electronic systems for a variety of functional devices.

Methods

Materials

Photoresin (B9R-2-Black Resin) was obtained from B9Creations. Diluent (Ebecryl 113) was obtained from Allnex. PVA (CAS:9002-89-5, average molecular weight 20,000–30,000) was obtained from Thermo Scientific. Gallium and indium (99.99% purity) were obtained from Luceteria Inc.

Fabrication of LM-STAIR vias

Detailed fabrication information is described in the Supplementary Note.

Physical characterization

A universal testing machine (Instron, cat no. 5944) was used to measure the mechanical properties. Electromechanical characterization was performed on a linear stage with a servo motor. The specimen was cut into a dog-bone geometry with dimensions specified in Fig. 3a. Electrical measurements were performed with a source measurement unit (Keithley 2461). For the demonstration, a d.c. supply is used to power the LED (MX3AWT-A1-0000-000E50, CreeLED, Inc.) and Hall effect sensor (A1326LLHLT-T, Allegro MicroSystems) circuitry. The dielectric constant was measured using the BK precision 880 Handheld LCR Meter with four different frequencies; 100 Hz, 1 kHz, 10 kHz and 100 kHz. The sample was prepared with a 1 cm circle shape and a thickness of 0.3 mm.

microCT scan

MicroCT was performed on LM composite samples that were manually trimmed from a dog-bone-shaped sample and placed on a Kapton with an energy of 60 kV and a resolution of 1.57 µm per voxel (Skyscan 1172 MicroCT scanner). Manual trimming can result in slight differences in sample dimensions, as seen in Fig. 2f, but it does not affect percolation and subsequent sample analysis. The image stack of the reconstructed slides was imported into Avizo software and then threshold segmented to visualize the 3D volume of the LM. The colour rendering of the LM phase was performed using the open-source software Blender.

Data availability

The data that support the findings of this study are available from the corresponding author upon reasonable request.

References

1. Mack, C. A. Fifty years of Moore's law. *IEEE Trans. Semicond. Manuf.* **24**, 202–207 (2011).
2. Lancaster, A. & Keswani, M. Integrated circuit packaging review with an emphasis on 3D packaging. *Integration* **60**, 204–212 (2018).
3. Gambino, J. P., Adderly, S. A. & Knickerbocker, J. U. An overview of through-silicon-via technology and manufacturing challenges. *Microelectron. Eng.* **135**, 73–106 (2015).
4. Hensleigh, R. et al. Charge-programmed three-dimensional printing for multi-material electronic devices. *Nat. Electron.* **3**, 216–224 (2020).
5. Rich, S. I., Wood, R. J. & Majidi, C. Untethered soft robotics. *Nat. Electron.* **1**, 102–112 (2018).
6. Truby, R. L., Katzschmann, R. K., Lewis, J. A. & Rus, D. Soft robotic fingers with embedded ionogel sensors and discrete actuation modes for somatosensitive manipulation. In *Proc. 2019 2nd IEEE International Conference on Soft Robotics (RoboSoft)* (ed Ren, H.) 322–329 (IEEE, 2019).
7. Bhattacharya, S. et al. A chest-conformable, wireless electro-mechanical e-tattoo for measuring multiple cardiac time intervals. *Adv. Electron. Mater.* **9**, 2201284 (2023).
8. Kim, D.-H. et al. Epidermal electronics. *Science* **333**, 838–843 (2011).

9. Guo, R. et al. Ni-gain amalgams enabled rapid and customizable fabrication of wearable and wireless healthcare electronics. *Adv. Eng. Mater.* **20**, 1800054 (2018).
10. Yao, D. et al. Achieving the upper bound of piezoelectric response in tunable, wearable 3D printed nanocomposites. *Adv. Funct. Mater.* **29**, 1903866 (2019).
11. Zhang, H. & Rogers, J. A. Recent advances in flexible inorganic light emitting diodes: from materials design to integrated optoelectronic platforms. *Adv. Opt. Mater.* **7**, 1800936 (2019).
12. Park, S., Vosguerichian, M. & Bao, Z. A review of fabrication and applications of carbon nanotube film-based flexible electronics. *Nanoscale* **5**, 1727–1752 (2013).
13. Sekitani, T. et al. Stretchable active-matrix organic light-emitting diode display using printable elastic conductors. *Nat. Mater.* **8**, 494–499 (2009).
14. Slee, D., Stepan, J., Wei, W. & Swart, J. Introduction to printed circuit board failures. In *Proc. 2009 IEEE Symposium on Product Compliance Engineering, PSES 2009* (ed Nix, D.) 1–8 (IEEE, 2009).
15. Kim, T. W., Lee, J. S., Kim, Y. C., Joo, Y. C. & Kim, B. J. Bending strain and bending fatigue lifetime of flexible metal electrodes on polymer substrates. *Materials* **12**, 2490 (2019).
16. Byun, J. et al. A single droplet-printed double-side universal soft electronic platform for highly integrated stretchable hybrid electronics. *Adv. Funct. Mater.* **27**, 1701912 (2017).
17. Shamkhalichenar, H., Bueche, C. J. & Choi, J. W. Printed circuit board (PCB) technology for electrochemical sensors and sensing platforms. *Biosensors* **10**, 159 (2020).
18. Zhang, Y., An, M., Yang, P. & Zhang, J. Recent advances in electroplating of through-hole copper interconnection. *Electrocatalysis* **12**, 619–627 (2021).
19. Dow, W.-P. et al. Through-hole filling by copper electroplating. *J. Electrochem. Soc.* **155**, D750 (2008).
20. Khoshmanesh, K. et al. Liquid metal enabled microfluidics. *Lab Chip* **17**, 974–993 (2017).
21. Bartlett, M. D. et al. High thermal conductivity in soft elastomers with elongated liquid metal inclusions. *Proc. Natl Acad Sci. USA* **114**, 2143–2148 (2017).
22. Dickey, M. D. et al. Eutectic gallium-indium (egain): a liquid metal alloy for the formation of stable structures in microchannels at room temperature. *Adv. Funct. Mater.* **18**, 1097–1104 (2008).
23. Veerapandian, S. et al. Hydrogen-doped viscoplastic liquid metal microparticles for stretchable printed metal lines. *Nat. Mater.* **20**, 533–540 (2021).
24. Zheng, Y. et al. Lignin-based encapsulation of liquid metal particles for flexible and high-efficiently recyclable electronics. *Adv. Funct. Mater* **34**, 2310653 (2024).
25. Dickey, M. D. Stretchable and soft electronics using liquid metals. *Adv. Mater.* **29**, 1606425 (2017).
26. Wang, X. & Liu, J. Recent advancements in liquid metal flexible printed electronics: properties, technologies, and applications. *Micromachines* **7**, 206 (2016).
27. Chen, S., Cui, Z., Wang, H., Wang, X. & Liu, J. Liquid metal flexible electronics: past, present, and future. *Appl. Phys. Rev.* **10**, 21308 (2023).
28. Ford, M. J., Patel, D. K., Pan, C., Bergbreiter, S. & Majidi, C. Controlled assembly of liquid metal inclusions as a general approach for multifunctional composites. *Adv. Mater.* **32**, 2002929 (2020).
29. Haque, A. T. et al. Electrically conductive liquid metal composite adhesives for reversible bonding of soft electronics. *Adv. Funct. Mater.* **34**, 2304101 (2023).
30. Lee, W. et al. Universal assembly of liquid metal particles in polymers enables elastic printed circuit board. *Science* **378**, 637–641 (2022).
31. Wu, D. et al. Fast and facile liquid metal printing via projection lithography for highly stretchable electronic circuits. *Adv. Mater.* **36**, 2307632 (2024).
32. Liu, S. et al. Ultrasonic-enabled nondestructive and substrate-independent liquid metal ink sintering. *Adv. Sci.* **10**, 2301292 (2023).
33. Yun, G. et al. Electro-mechano responsive elastomers with self-tunable conductivity and stiffness. *Sci. Adv.* **9**, eadf1141 (2023).
34. Kim, M. G., Alrowais, H., Pavlidis, S. & Brand, O. Size-scalable and high-density liquid-metal-based soft electronic passive components and circuits using soft lithography. *Adv. Funct. Mater.* **27**, 1604466 (2017).
35. Ren, P. & Dong, J. Direct fabrication of via interconnects by electrohydrodynamic printing for multi-layer 3d flexible and stretchable electronics. *Adv. Mater. Technol.* **6**, 2100280 (2021).
36. Marques, D. G., Lopes, P. A., de Almeida, A. T., Majidi, C. & Tavakoli, M. Reliable interfaces for egain multi-layer stretchable circuits and microelectronics. *Lab Chip* **19**, 897–906 (2019).
37. Liu, S., Shah, D. S. & Kramer-Bottiglio, R. Highly stretchable multilayer electronic circuits using biphasic gallium-indium. *Nat. Mater.* **20**, 851–858 (2021).
38. Hirsch, A. et al. Intrinsically stretchable biphasic (solid-liquid) thin metal films. *Adv. Mater.* **28**, 4507–4512 (2016).
39. Yoon, J. et al. Design and fabrication of novel stretchable device arrays on a deformable polymer substrate with embedded liquid-metal interconnections. *Adv. Mater.* **26**, 6580–6586 (2014).
40. Franssila, S. *Introduction to Microfabrication* (Wiley, 2010).
41. Patel, D. K. et al. Highly stretchable and UV curable elastomers for digital light processing based 3D printing. *Adv. Mater.* **29**, 1606000 (2017).
42. Qi, D., Zhang, K., Tian, G., Jiang, B. & Huang, Y. Stretchable electronics based on PDMS substrates. *Adv. Mater.* **33**, 2003155 (2021).
43. Llerena Zambrano, B. et al. Soft electronics based on stretchable and conductive nanocomposites for biomedical applications. *Adv. Healthc. Mater.* **10**, 2001397 (2021).
44. Bartlett, M. D. et al. Stretchable, high-k dielectric elastomers through liquid-metal inclusions. *Adv. Mater.* **28**, 3726–3731 (2016).
45. Style, R. W. et al. Stiffening solids with liquid inclusions. *Nat. Phys.* **11**, 82–87 (2015).
46. Markvicka, E. J., Bartlett, M. D., Huang, X. & Majidi, C. An autonomously electrically self-healing liquid metal–elastomer composite for robust soft-matter robotics and electronics. *Nat. Materials* **17**, 618–624 (2018).
47. Ford, M. J. et al. A multifunctional shape-morphing elastomer with liquid metal inclusions. *Proc. Natl Acad. Sci. USA* **116**, 21438–21444 (2019).
48. Baum, D. et al. High-throughput segmentation of tiled biological structures using random-walk distance transforms. *Integr. Comp. Biol.* **59**, 1700–1712 (2019).
49. Cheng, N.-S. Simplified settling velocity formula for sediment particle. *J. Hydraul. Eng.* **123**, 149–152 (1997).
50. Bogatin, E. Essential principles of signal integrity. *IEEE Microw. Mag.* **12**, 34–41 (2011).
51. Liu, Y. et al. Synthesis and applications of low dielectric polyimide. *Resour. Chem. Mater.* **2**, 49–62 (2023).
52. Barron III, E. J., Williams, E. T., Wilcox, B. T., Ho, D. H. & Bartlett, M. D. Liquid metal-elastomer composites for water-resilient soft electronics. *J. Polymer Sci.* https://doi.org/10.1002/pol.20230616 (2023).

Acknowledgements

D.H.H. and M.D.B. acknowledge support from the Office of Naval Research Young Investigator Program (ONR YIP) (grant no. N000142112699) and the National Science Foundation CAREER

award (grant no. 2238754). C.H. and L.L. acknowledge support from Virginia Polytechnic Institute and State University through the COE Faculty Fellowship. C.H. and L.L. also thank D. Baum for the kind assistance in using random-work distance transforms for quantitative microCT analysis.

Author contributions

D.H.H. and M.D.B. conceived and designed research. D.H.H. conducted research. C.H. and L.L. contributed to measurement and analysis of the microCT scan data. M.D.B. supervised the work. D.H.H. and M.D.B. wrote the paper with contributions from all the authors.

Competing interests

M.D.B. and D.H.H. are inventors on a patent application (US Patent Application no. 63/535,919) on the fabrication approach. The other authors declare no competing interests.

Additional information

Supplementary information The online version contains supplementary material available at https://doi.org/10.1038/s41928-024-01268-z.

Correspondence and requests for materials should be addressed to Michael D. Bartlett.

Peer review information *Nature Electronics* thanks Wedyan Babatain, Sungjune Park and Nanjia Zhou for their contribution to the peer review of this work.

Reprints and permissions information is available at www.nature.com/reprints.

Publisher's note Springer Nature remains neutral with regard to jurisdictional claims in published maps and institutional affiliations.

Springer Nature or its licensor (e.g. a society or other partner) holds exclusive rights to this article under a publishing agreement with the author(s) or other rightsholder(s); author self-archiving of the accepted manuscript version of this article is solely governed by the terms of such publishing agreement and applicable law.

© The Author(s), under exclusive licence to Springer Nature Limited 2024, corrected publication 2024